FAILURE ANALYSIS OF ROTARY KILN'S TERTIARY AIR DUCTS *

Cleber Caetano Thomazi[1]
Yuri Castilho Caldeira Brant[2]
Baltazar Agenor Bailona[3]
Hamilton Lelis Ito[4]
Osvaldo da Silva Neto[5]

Abstract
Rotary kilns are continuous process equipment used on calcining of nickel ore. The chemical and physical reactions are created by means of heat up the material to predetermined temperatures. Tertiary air fans are attached to the kiln shell to maintain oxidizing/reduction conditions. Special ducts orientate the air flow inside the kiln. In the present work, two types of failure on distinct tertiary ducts mounted on the same kiln are reported. Chemical analysis, hardness test, metallographic and fractographic examinations were carried out. Fabrication related problems and creep were identified as the root causes of damages.
Keywords: Kiln; Tertiary air ducts; Casting defects; Creep.

1 *Mechanical Engineer/Sc.D., Reliability Engineer, Maintenance Engineering, Anglo American, Barro Alto, Goiás, Brazil.*
2 *Mechanical Engineer/BSc, Reliability Engineer, Maintenance Engineering, Anglo American, Barro Alto, Goiás, Brazil.*
3 *Mechanical Engineer/M.S., Engineering Coordinator, Maintenance Engineering, Anglo American, Barro Alto, Goiás, Brazil.*
4 *Metallurgical Engineer/ Sc.D., Researcher, FIPT, Instituto de Pesquisas Tecnológicas, São Paulo, São Paulo, Brazil.*
5 *Materials Engineer/BSc, Product and Process Engineering Coordinator, Department of Engineering, USIPE, Içara, Santa Catarina, Brazil.*

1 INTRODUCTION

Rotary kiln (RK) is of the utmost importance on the production of iron-nickel (Fe-Ni) by means of pyrometallurgical process. Its objective is to produce a high quality calcine to the electric furnace (EF). A high level of reduction of the iron and nickel oxides, an elevated temperature, a minimum quantity of fines and gases emissions are calcine properties that ensure a stable and smooth EF smelting operation and minimize the energy consumption.

The retention time of the calcine at elevated temperatures shall be as long as possible to achieve the operational goals. These can be achieved by: (a) a counter flow of hot gas and cold moist feed; (b) a controlled use of sub-stoichiometric combustion (at the maximum allowable temperature) and (c) a post-combustion of reduction gases. The sub-stoichiometric conditions and the use of tertiary air fans for post-combustion are responsible for the extended temperature profile and to improve the reduction potential. The combustion of the monoxide carbon contained in the process gas by the injection of tertiary air into the RK releases additional heat to the calcine [1].

Anglo American Barro Alto nickel plant has two RK with following dimensions 6.1 m x 7.0 m diameter x 185 m long. Each one has a series of four tertiary air fans located on the kiln shell. Figure 1 shows the portion of the RK #2 (412-FC-002) with the location of the tertiary air fans (412-VE-008, 009, 010 and 011). The air flow is introduced and oriented into the RK by means of pipes termed “tertiary air ducts” (Figures 1.b and 1.c).

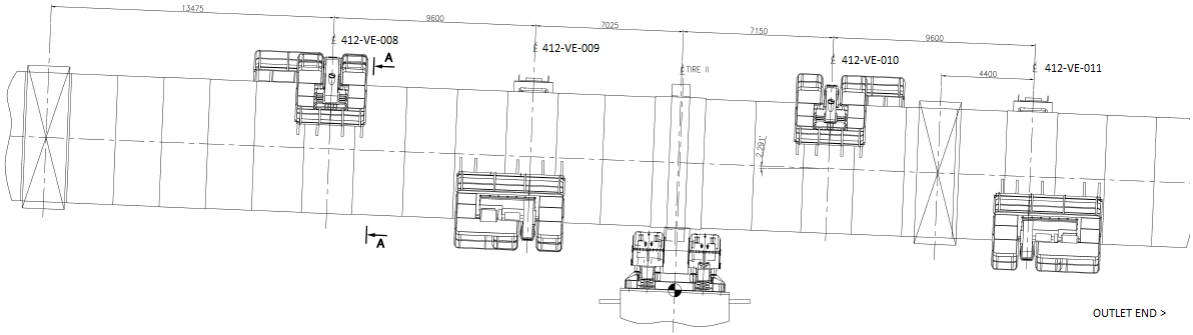

(a)

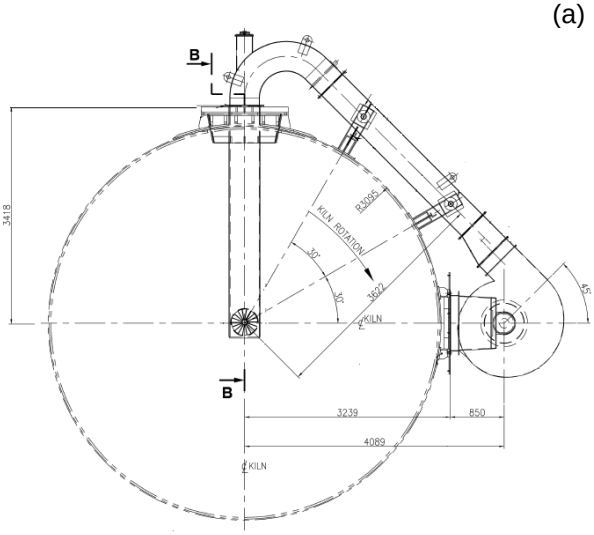

A-A

(b)

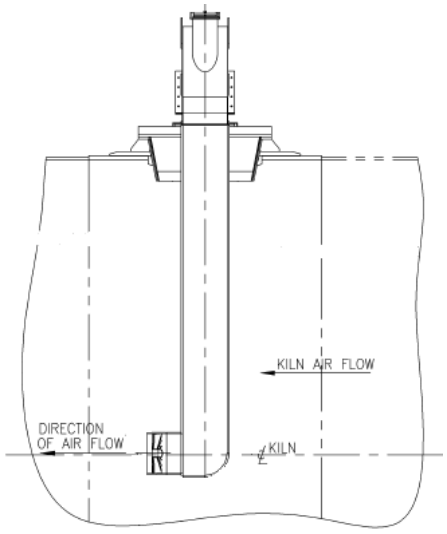

B-B

(c)

Figure 1. (a) Tertiary air fans along the RK #2 shell; (b) section A-A; (c) section (B-B). After [2].

The tertiary air ducts are subject to various failure mechanisms: creep, fatigue, corrosion, abrasive wear and fracture. The recent history of ducts failures and the reasons they were taken out of service for both RK are presented in Table 1. According to the operating team, the average service life of these components is approximately one year.

Table 1. Recent history of failures of the tertiary air ducts.

Equipment		Date			
		10/20/2016	12/27/2016	01/27/2016	02/15/2017
RK#1 411-FC-001	411-VE-008				
	411-VE-009			warped	
	411-VE-010			fractured	
	411-VE-011				
RK#2 412-FC-001	412-VE-008				
	412-VE-009		warped		
	412-VE-010	warped	fractured		warped
	412-VE-011				

This work presents the failure analysis of the 412-VE-009 and 412-VE-010 ducts, shown in Figure 2. Both failures were detected in 12/27/2016. The results of tests and examinations reported here are based on [3].

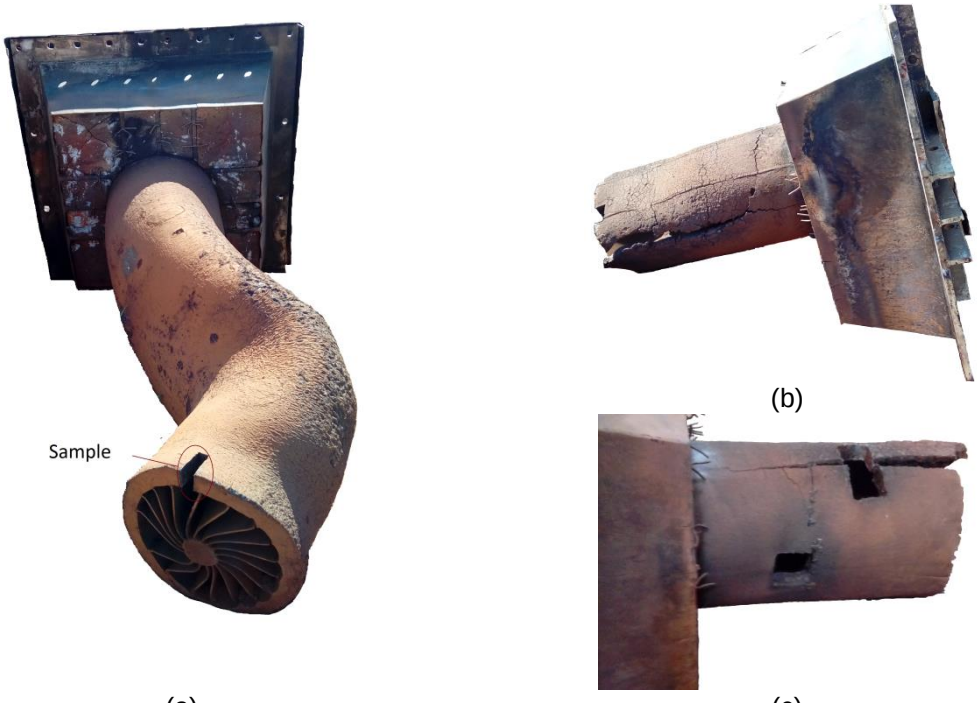

Figure 2. Tertiary ducts: (a) 412-VE-009; (b) and (c) 412-VE-010.

2 MATERIAL AND METHODS

2.1 Sampling and Methodology

Three samples were taken from the fractured duct (412-VE-010). They were identified as M4719-1, M4719-2 and M4719-3. The warped duct had one sample extracted from (M4719-4). Figure 2 also shows the locations from where the samples were taken.

For the accomplishment of chemical analyzes, hardness tests, fractographic and metallographic examinations, test specimens from the samples were extracted. Figure 3 presents the samples, while Table 2 shows the list of the examinations and tests carried out, the test specimens' locations and the identification adopted.

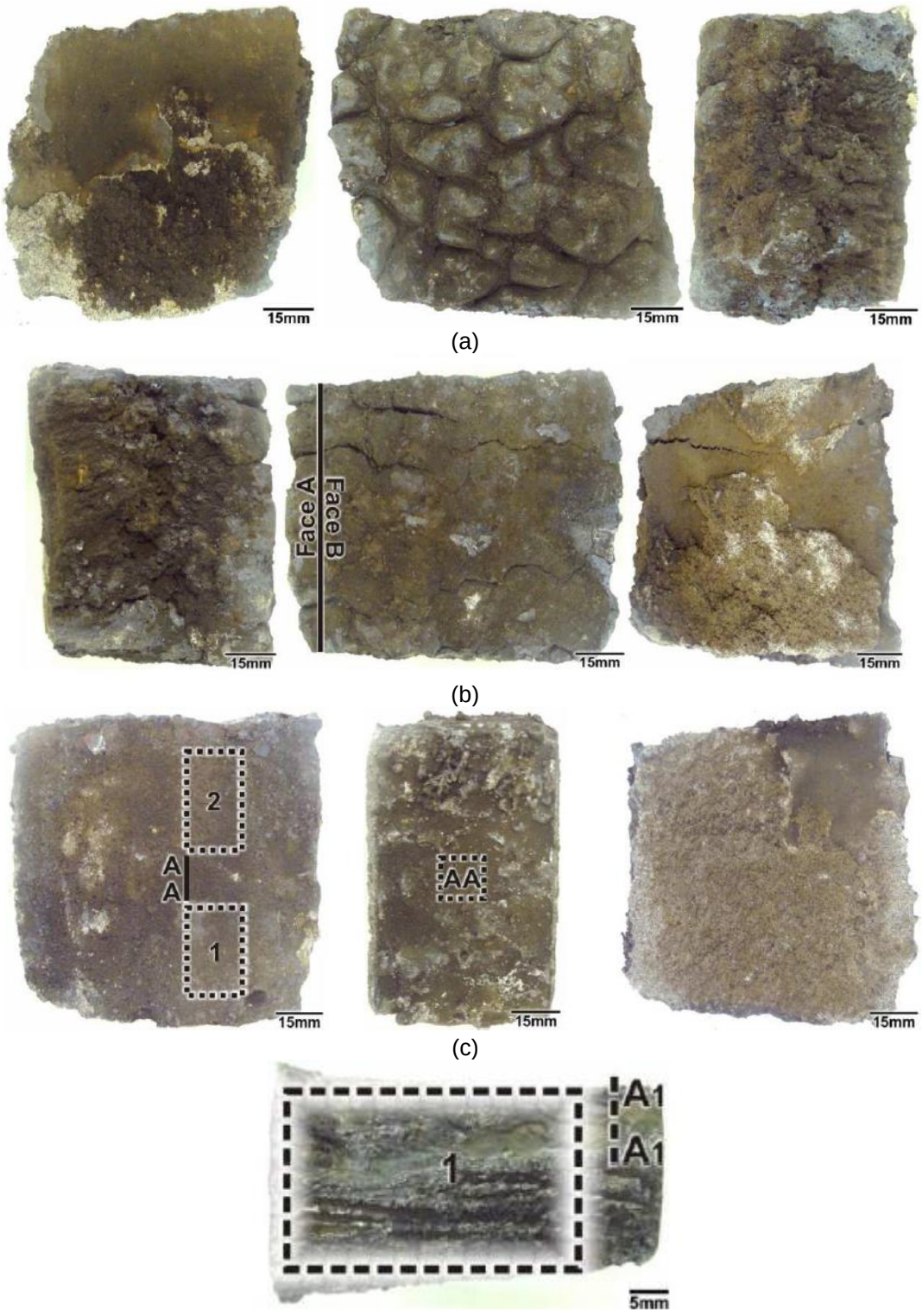

Figure 3. (a) Sample #1; (b) sample #2; (c) sample #3; (d) sample #4. After [3].

Table 2. List of tests and examinations with the respective samples, regions and sections considered for analyzes and test specimens' identification.

Test or analysis	Sample	Region	Section	Specimen ID
Chemical analysis	3	1		M4719-1
Brinell hardness	3	2		M4719-2
Fractographic exam	2	1		M4719-3
Micrographic exam	3		A-A	M4719-4
Chemical analysis and hardness test	4	1		M4719-5
Micrographic exam	4		A_1-A_1	M4719-6

After [3].

The combustion method was used for the chemical analyzes of the carbon and sulfur elements, while the plasma atomic emission spectrometry method was applied to the other elements. The Standard Test Methods ASTM E1019-11 [4] and ASTM E350:12 [5] were adopted for these analyzes, respectively. The following equipment were used: Carbon and Sulfur Analyzer, model CS-300 (LECO); Plasma Atomic Emission Spectroscopy (ICP), model Vista MPX (VARIAN).

The fractographic examinations were performed in sample 2 according to the IPT 10846 internal procedure, *apud* [3]. For these tests, the specimens were submitted to ultrasonic cleaning in alcohol for 10 minutes. The macrofractographic examinations were recorded with a Sony DSC HX100 digital camera. The microfractographic examinations were conducted in a FEI QUANTA 400 scanning electron microscope (SEM). The SEM images were obtained with a 15 kV acceleration voltage and current of approximately 1 nA. The images presented were obtained with the secondary electron detector and backscattered electron detector.

The micrographs were performed with an Olympus BX51M optical microscope, according to the IPT 10844 procedure, *apud* [3]. Chemical attack by ferric chloride was used for etching.

The Brinell hardness tests in the specimen M4719-2 were carried out with a load of 29421 N and a 10 mm diameter tungsten carbide ball indenter in a Wilson Model J tester, according to the IPT 10847 procedure, *apud* [3]. Due to the sample size limitations, the Brinell hardness tests on the specimen M4719-5, extracted from sample #4, were performed with a load of 1838.75 N and a 2.5 mm diameter tungsten carbide ball in a Heckert WPM testing machine, according to the IPT 10847 procedure, *apud* [3]. As results, the mean and standard deviation values of five hardness measurements were presented.

As the chemical composition of the ducts' materials does not match with any known commercial alloy presented in the technical literature, a thermodynamic simulation was carried out using the Thermo-calc software to obtain a better understand of the observed microstructures.

3 RESULTS AND DISCUSSION

3.1 Chemical Analyzes

The results of the chemical analyzes are reproduced in Table 3. It can be seen that the ducts were made from ferrous alloys containing about 23 % chromium, 6 % cobalt and 1.5 % manganese. The carbon content differs greatly between the samples.

Table 3. Chemical composition.

Element	Specimen M4719-1, %	Specimen M4719-5, %
Carbon (C)	0.57 ± 0.01	0.18 ± 0.01
Silicon (Si)	0.68 ± 0.01	0.79 ± 0.01
Manganese (Mn)	1.42 ± 0.01	1.44 ± 0.01
Phosphorus (P)	0.019 ± 0.001	0.039 ± 0.001
Sulfur (S)	0.006 ± 0.001	0.004 ± 0.001
Chromium (Cr)	22.2 ± 0.3	23.0 ± 0.3
Nickel (Ni)	0.30 ± 0.02	0.40 ± 0.02
Molybdenum (Mo)	0.019 ± 0.001	0.021 ± 0.002
Cobalt (Co)	6.3 ± 0.1	6.1 ± 0.1
Iron (Fe)	Balance	Balance

After [3]. 95 % confidence interval for the mean of a sample size of 3.

3.2 Hardness Tests

Table 4 shows the average and the standard deviations obtained in the hardness tests performed in the fractured (M4719-2) and warped (M4719-5) ducts samples.

Table 4. Brinell hardness.

	Sample M4719-2	Sample M4719-5
Average	376	249
Standard deviation	33	5

After [3].

3.3 Visual and Fractographic Examinations

The surface aspect of samples #1 and #2 (Figure 4.a and 5.a) is compatible with damage caused by oxidation at high temperature.
Figure 4.a shows the sample #1 sectioning plans. The arrow I points to the fractured surface, while arrows II and III point to the sectioned surfaces presented in detail in Figures 4.b and 4.c, respectively. The sections revealed cracks and the presence of voids in the central region of the sample. The morphology and position of these voids indicate a casting defect known as shrinkage, resulting from the liquid-solid contraction that the material underwent during solidification.

(a) (b) (c)

Figure 4. (a) Sample #1; (b) and (c) sections indicated by arrows II and III respectively. After [3].

Figure 5.a shows sectioning plan of sample #2. The arrow I points to the fractured surface. The arrow II points to the sectioned surface presented in Figure 5.b, in which can be observed cracks, high temperature oxidation regions and shrinkages in the central region. These voids are larger than those observed in sample #1. The extent

of the defect was so great that a small impact load in the sample was sufficient to fragment it into four parts (Figure 5.c).

(a) (b) (c)

Figure 5. (a) Sample #2; (b) section indicated by arrow I; (c) the same section after a little impact load. After [3].

Specimens taken from the regions with voids of sample #2 were subjected to observation on the SEM. The results are shown in Figure 6. It can be seen dendrites resulting from the solidification and confirmed that defects in the extracted samples of the fractured duct are shrinkages.

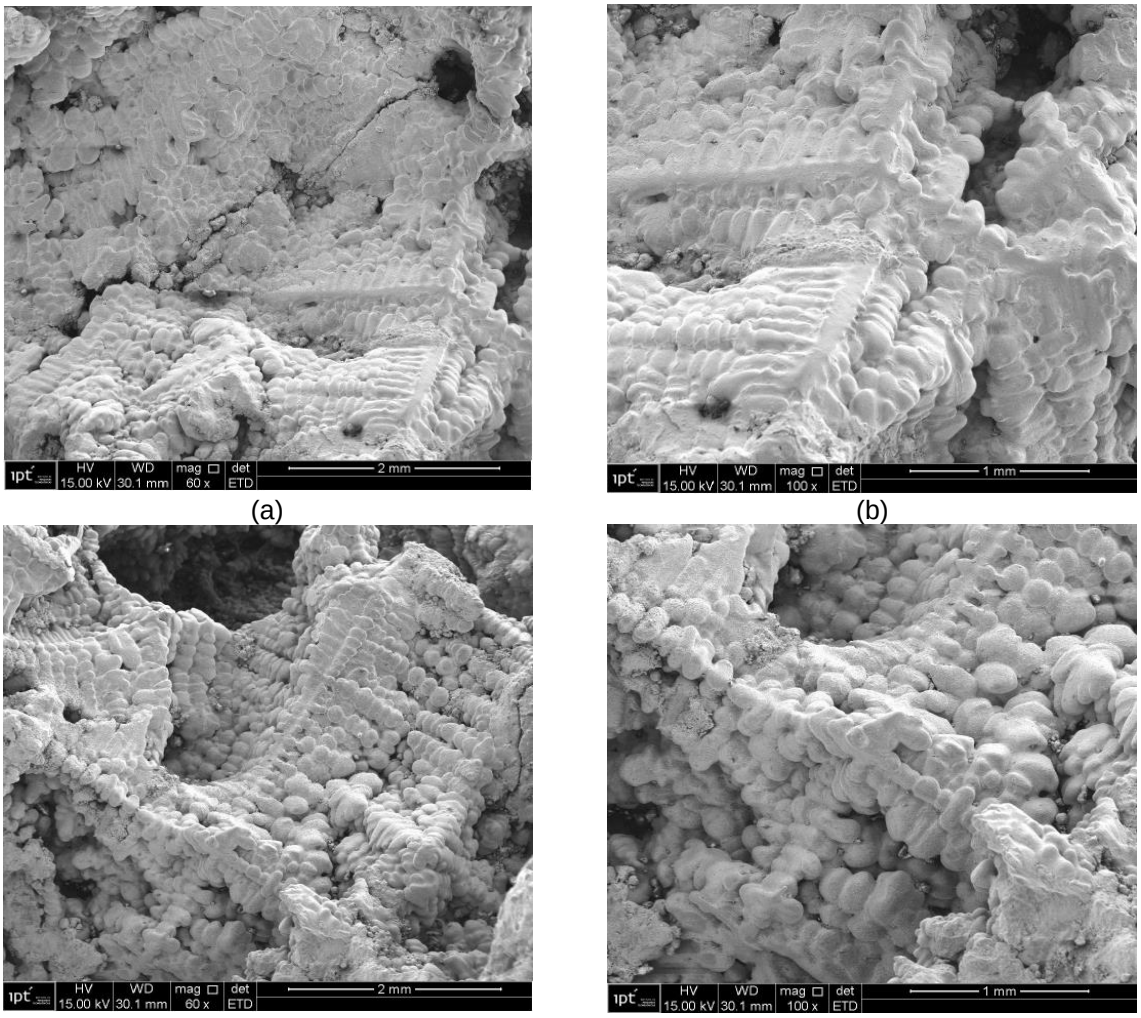

(a) (b) (c) (d)

Figure 6. Surface topographic appearance of the voids observed in sample #2, specimen M4719-3: (a) and (b) region 1; (c) and (d) region 3. After [3].

3.4 Metallographic Examinations

The metallographic analysis of the fractured duct material (sample #3) revealed characteristic microstructure of a cast hypoeutectic ferrous alloy, showing carbides in interdendritic regions and secondary carbides precipitation in the matrix (Figure 7). The chemical composition and the ferromagnetic nature observed in the alloy indicate that the material has a ferritic matrix. The same test specimen for the results of Figure 7 was observed on the SEM. Figure 8 shows backscattered electron images and secondary electron images of the microstructure of this material.

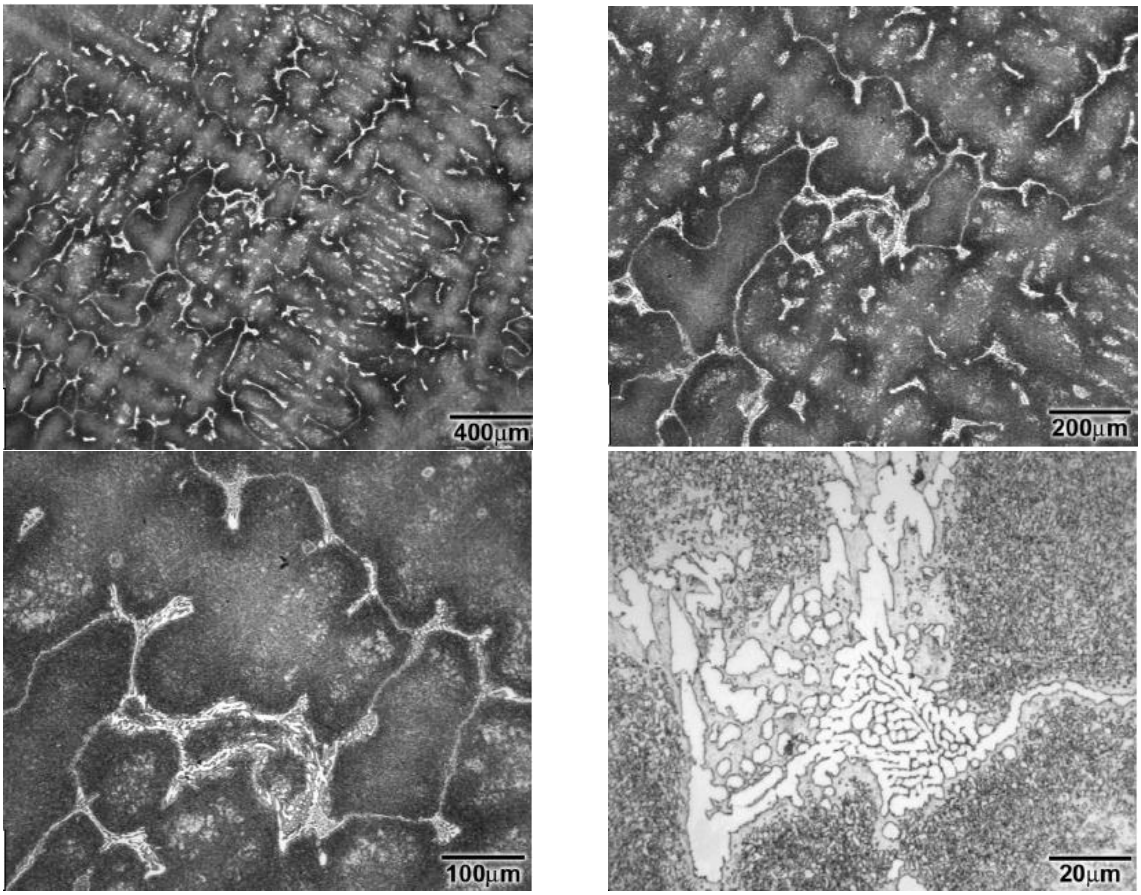

Figure 7. Test specimen M4719-4 microstructure observed with increasing magnitudes. After [3]

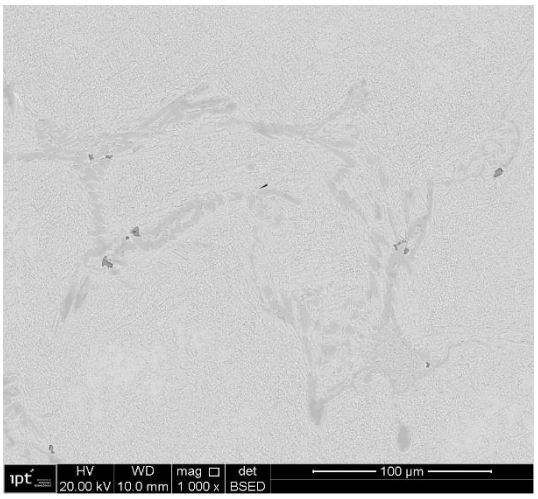

(a)

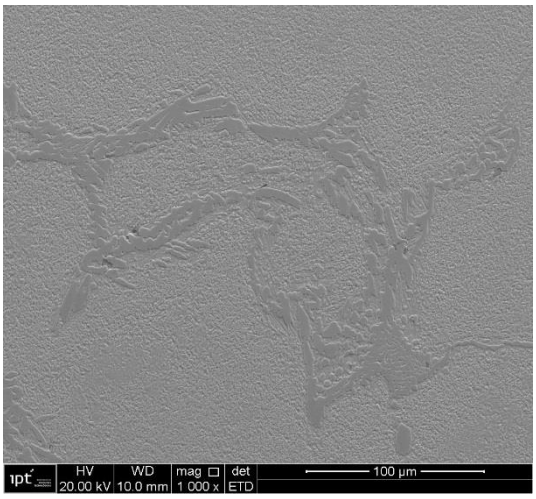

(b)

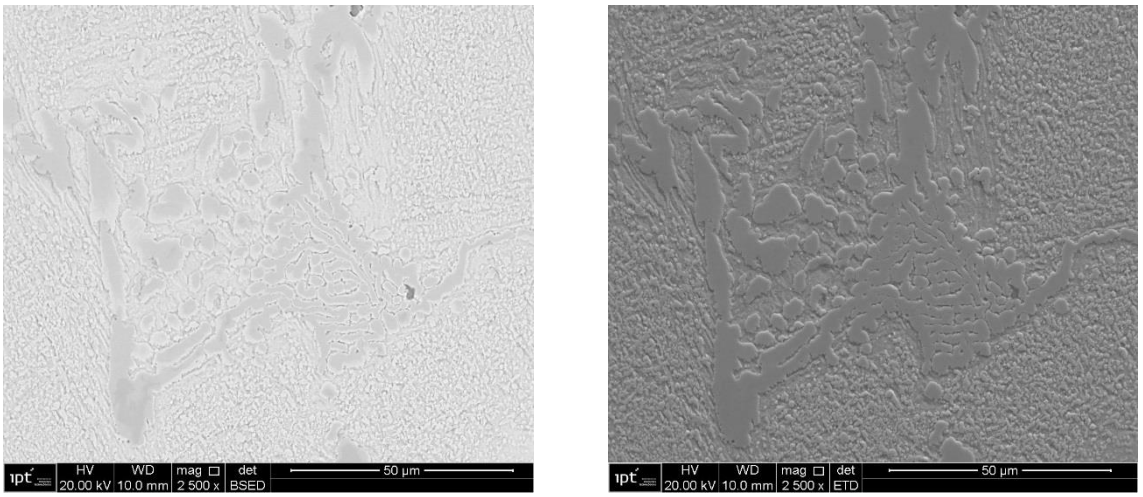

(c) (d)

Figure 8. (a) Image of backscattered electrons showing the interdendritic eutectic region; (b) the same region of (a) observed with secondary electron image; (c) backscattered electron beam showing the interdendritic eutectic region with the highest magnification; (d) the same region of (c) observed with secondary electron image. Sample #3 - test specimen M4719-4. After [3].

Microstructural analysis of the warped duct material (sample #4) revealed microstructure of a cast ferrous alloy (Figure 9). In this sample the presence of eutectic microconstituents was not observed. The morphology of the dark microconstituent suggests being precipitates resulting from reaction in the solid state known as discontinuous precipitation. The same test specimen with respect to the results of Figure 9 was observed on the SEM. Figure 10 shows backscattered electron images and secondary electron images of the microstructure of the material.

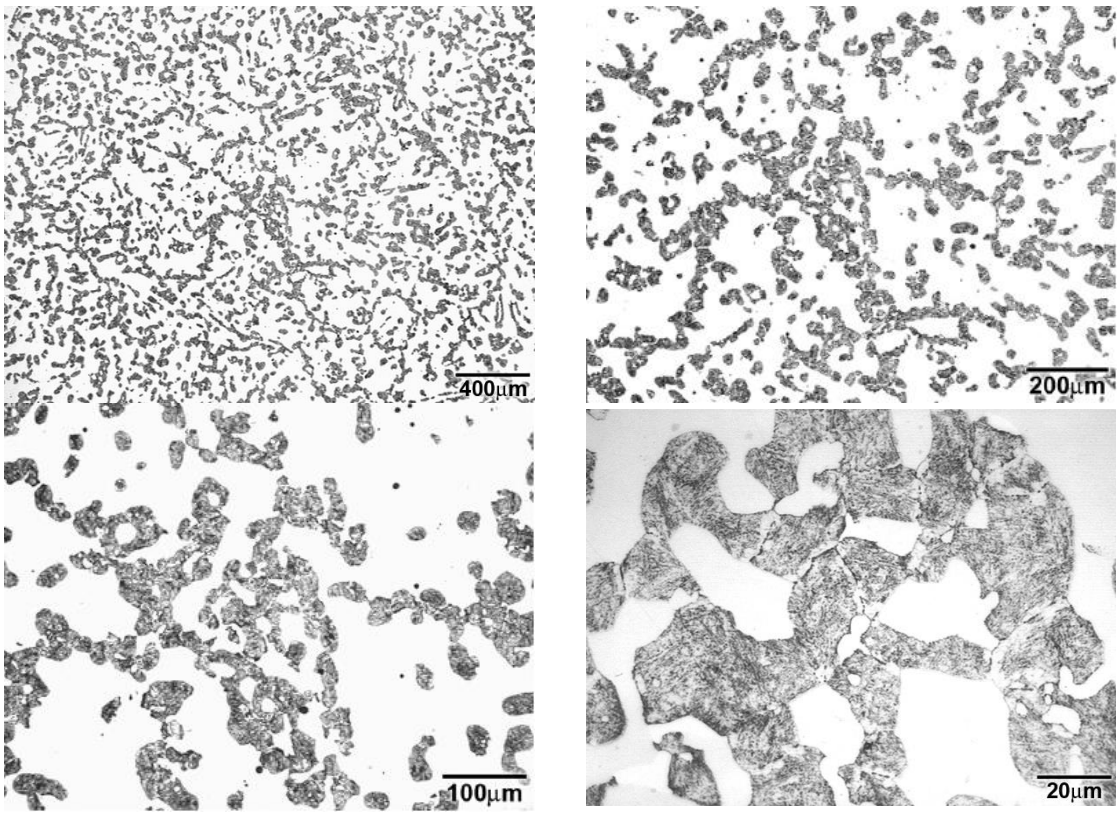

Figure 9. Aspect of sample #4 – test specimen M4719-6 microstructure observed with increasing magnitudes. After [3].

The lamellar nature of the carbides is clearly observed in Figure 10.d; this is a typical characteristic of as discontinuous precipitation.

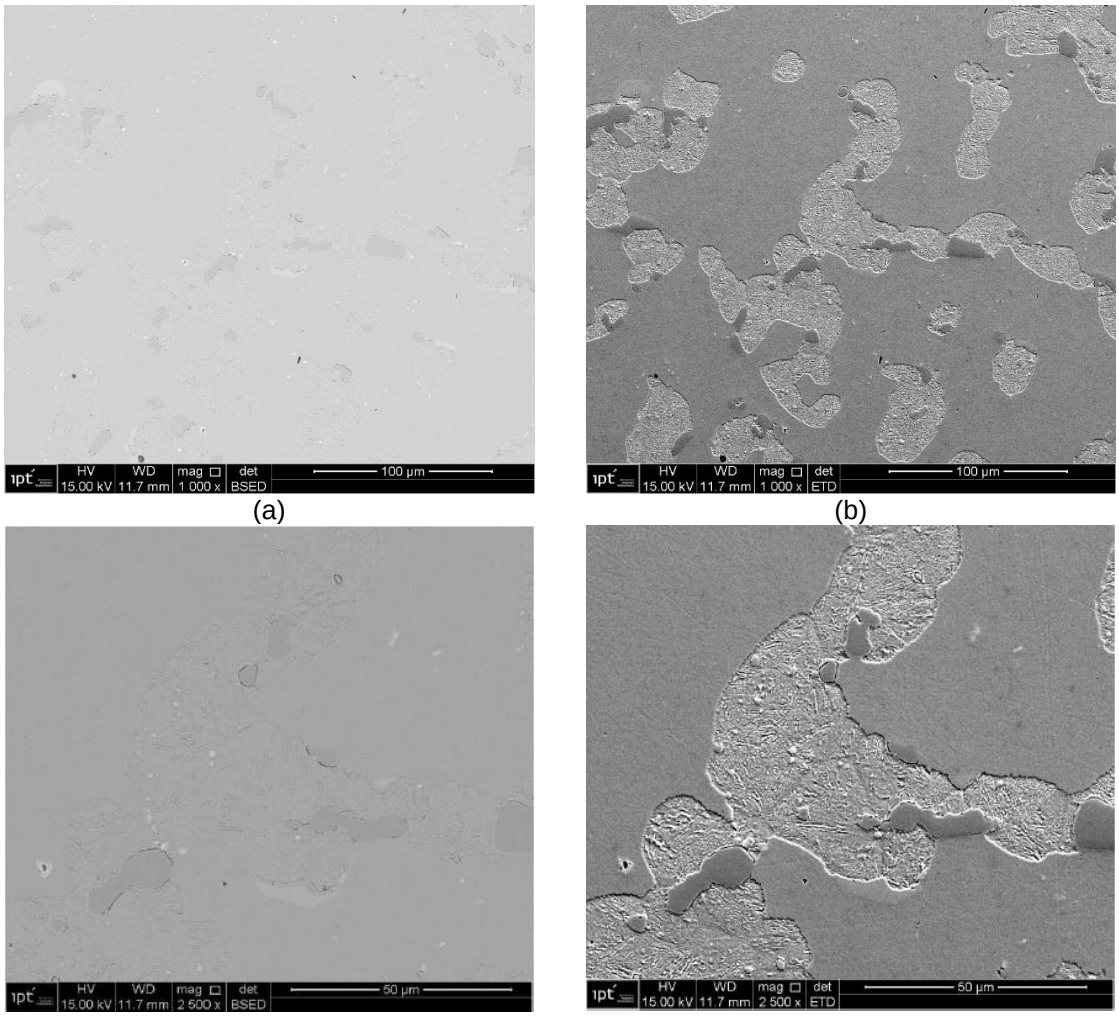

Figure 10. (a) Backscattered electrons image showing areas with different shades of gray; (b) same region of (a) observed with secondary electron image; (c) backscattered electrons image showing the same region of (a) with higher magnification; (d) same region of (c) observed with secondary electron image. Sample #4 – test specimen M4719-6. After [3].

3.5 Further Discussion

The chemical compositions of the fractured and deformed ducts materials differs on the carbon contents but are similar with respect to other elements such as chromium and cobalt. It indicates that the manufacturing process is not completely under control. No similar alloy was identified in the specialized literature [6, 7].

Figure 11 presents the equilibrium pseudo-binary phase diagram obtained by Thermo-calc software. The ducts were submitted to temperatures of almost 1000 °C.

For this temperature, the alloy with less carbon content presents the following equilibrium phases: ferrite (BCC_A2), austenite (FCC_A1) and secondary carbide ($M_{23}C_6$). It was observed no eutectic reaction for the alloy with 0.18 %C, which is compatible with the results of the metallographic analysis.

At equilibrium, and the temperature maintained at 1000 ºC, the alloy with 0.57 %C (fractured duct) presents austenite (FCC_A1) and the $M_{23}C_6$ secondary carbide phases. It can be note that in the solidification sequence of this alloy a ternary eutectic

reaction is expected with the formation of the M_7C_3 carbide and this carbide undergoes decomposition for $M_{23}C_6$. The carbides observed in interdendritic regions (Figures 7) are probably the carbides $M_{23}C_6$.

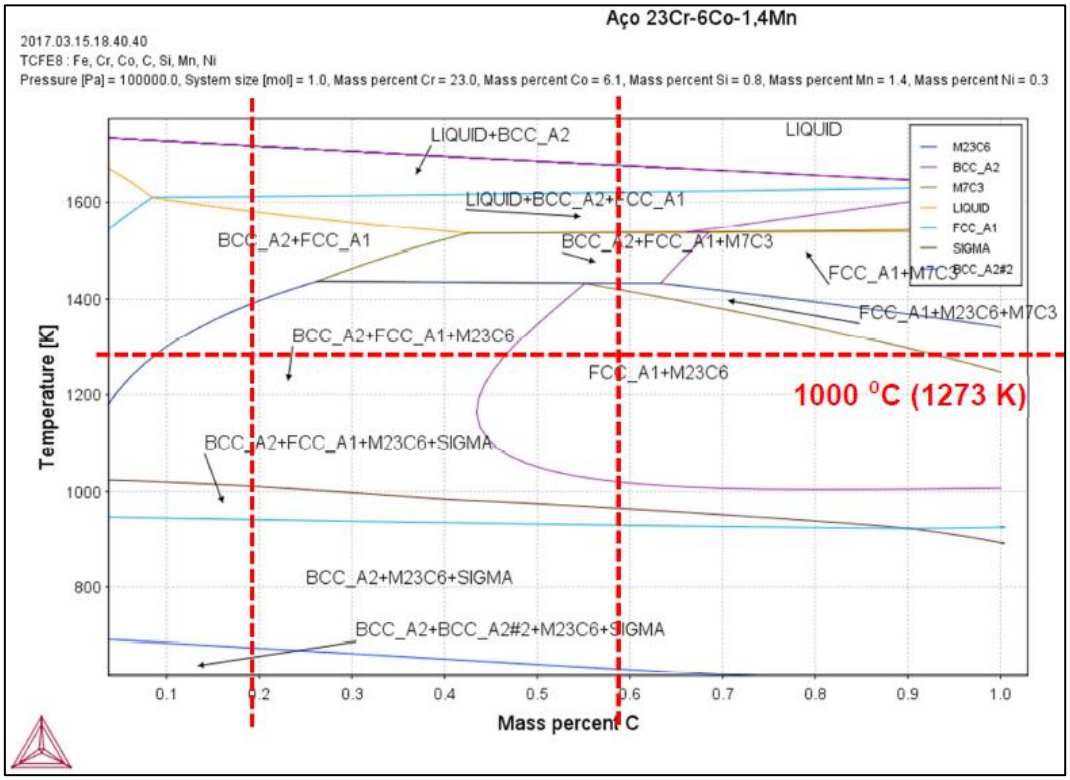

Figure 11. Pseudo-binary equilibrium diagram of a steel containing 23 % Cr, 6 % cobalt and 1.4 % manganese as a function of carbon content.

In the Figures 4 and 5 one may observe the metallurgical defects (shrinkage) that caused the premature fracture of the duct. The extension of these defects decreased the creep strength of the duct causing its premature failure.

The plastic deformation observed in the warped duct (Figure 2.a), is considered to be a consequence of creep under high temperature effect. Creep strength and oxidation resistance are critical properties in refractory or heat-resistant alloys. Keep air flowing inside the ducts is of primary importance for a long service life.

The specialized technical literature [6,7] presents families of heat-resistant alloys of Fe-Cr with chromium contents between 10 % and 30 %; Fe-Cr-Ni alloys with chromium contents greater than 13 % and Ni contents higher than 10 %, with Cr content greater than Ni content; Fe-Ni-Cr alloys with nickel contents greater than 25 % and chromium contents higher than 10 %, with nickel content greater than chromium; nickel-based alloys (Ni content ≥ 50 %); and cobalt-based alloys (Co content ≥ 50 %). As the chemical compositions of the two analyzed alloys did not fit into any of the alloy families mentioned above, it was decided to make use of the Sthalschlüssel [8] searching for alloys of proprietary compositions. No similar metal alloys were identified and, therefore, it was not possible to compare the creep strength of the analyzed materials with those foreseen in the literature for heat- resistant alloys.

4 CONCLUSIONS

The chemical compositions of the fractured and warped ducts are different in terms of carbon contents, but are similar with respect to the other elements. This fact indicates an out of control manufacturing process.
It was not possible to comprise the duct materials with any commercial heat-resistant alloy. It suggests that this alloy was developed specifically for Anglo American's kilns.
The premature failure of the fractured duct was attributed to the presence of casting defects, which affected negatively its strength, while the warped duct failed by creep. The presence of shrinkage in excess is also considered a lack of control in the manufacturing process.
Both ducts presented high temperature oxidation, a corrosion process expected for that environment.
The failure analysis presented in this paper led to a series of actions aimed obtaining a longer service life for the tertiary air ducts. A simulation of the casting process (filling, solidification, cooling and feeding system) was commissioned in order to prevent metal casting defects. Creep tests to identify the parameters that dictate the behavior of the specified duct material were also performed. These parameters were used in numerical simulations to compare the predicted life of the original duct with one manufactured with an H-type alloy [9]. Optimization of the duct geometry is in progress. The results of these studies will be published opportunely in a future article.

Acknowledgments

The authors would like to acknowledge the financial support received from Anglo American Brazil. The authors are also grateful to the technical staff of the Corrosion and Protection Laboratory - LCP / CTMM / IPT – for their support in analyzes.

REFERENCES

1 Anglo American. Process design criteria and description design criteria process. Barro Alto: Anglo American; 2009.
2 Flmidth Minerals. Kiln System - Installation, Operation, and Maintenance Manual. Vol. 3. Flsmidth; 2008.
3 IPT. Caracterização fractográfica de uma amostra de tubo de metal refratário e caracterização do material de amostras de metal refratário. Technical Report n. 150 007-205. São Paulo: Instituto de Pesquisas Tecnológicas; 2017 (in Portuguese).
4 ASTM. E1019-11, Standard Test Methods for Determination of Carbon, Sulfur, Nitrogen, and Oxygen in Steel, Iron, Nickel, and Cobalt Alloys by Various Combustion and Fusion Techniques. West Conshohocken: ASTM International; 2011.
5 ASTM. E350-12, Standard Test Methods for Chemical Analysis of Carbon Steel, Low Alloy Steel, Silicon, Electrical Steel, Ingot Iron, and Wrought Iron. West Conshohocken: ASTM International; 2012.
6 ASM. Metals Handbook - Properties and Selection: Stainless Steels, Tool Materials and Special Purpose Metals. Vol. 3. 9th Edition. Metals Park, OH: ASM International; 1980.
7 ASM. ASM Specialty Handbook: Heat-Resistant Materials. ASM International; 1997.
8 Verlag Stahlschlüssel Wegst. Sthalschlüssel – Key to steel. Computer program. Marbach: Verlag Stahlschlüssel; 2010.
9 ASTM. A297/A297M-10, Standard Specification for Steel Castings, Iron-Chromium and Iron-Chromium-Nickel, Heat Resistant, for General Application. West Conshohocken, PA: ASTM International; 2010.